Electronic Supplementary Material (ESI) for Materials Chemistry Frontiers.
This journal is © the Partner Organisations 2022

Supporting Information

Regulation of Excited-State Properties of Dibenzothiophene-Based Fluorophores for Realizing Efficient Deep-Blue and HLCT-Sensitized OLEDs

Jichen Lv[a], Yumiao Huo[d], Shu Xiao[b], Zhennan Zhao[c], Ling Peng[a], Yuchao Liu[a], Zhongjie Ren[c], Dongge Ma[b], Shian Ying[a, b*] and Shouke Yan[a, c*]

[a] Key Laboratory of Rubber-Plastics, Ministry of Education, Qingdao University of Science & Technology, Qingdao 266042, P. R. China.

[b] Institute of Polymer Optoelectronic Materials and Devices, State Key Laboratory of Luminescent Materials and Devices, South China University of Technology, Guangzhou 510640, P. R. China.

[c] State Key Laboratory of Chemical Resource Engineering, College of Materials Science and Engineering, Beijing University of Chemical Technology, Beijing 100029, P. R. China.

[d] College of Materials Science and Engineering, Shandong University of Science and Technology, Qingdao 266590, P. R. China.

*Corresponding author: shian0610@126.com; skyan@mail.buct.edu.cn

1. EXPERIMENTAL METHODS

1.1. Experimental measurements

^{1}H and ^{13}C nuclear magnetic resonance (NMR) spectra were performed by the Bruker AC500 spectrometer at 500 MHz and 125 MHz with $CDCl_3$ and tetramethylsilane (TMS) as the solvent and internal standard, respectively. Mass spectra of compound were measured by High Resolution Quadrupole Time of Flight Tandem Mass Spectrometer (TOF-MS). UV-visible absorption and emission spectra were carried out by using Hitachi U-4100 absorption spectrometer and Hitachi F-4600 spectrophotometer, respectively. Photoluminescence quantum yields (PLQYs) of materials in solution and film were estimated by using the integration sphere setup (Hamamatsu C11347-11) equipped with a xenon high-pressure lamp and a multichannel analyzer from 200 to 950 nm. Phosphorescence spectra of materials were measured at 77 K in dichloromethane solution after delay time of 1 ms by the Edinburgh FLS-980 with an EPL-340 optical laser. Thermogravimetric analysis (TGA) curves of materials were performed using a Netzsch (209F1) thermogravimetric analyzer under a nitrogen atmosphere (50 mL min^{-1}) at a heating rate of 10 ^{o}C min^{-1}. Differential scanning calorimetry (DSC) curves of target compounds were recorded by a Netzsch DSC (204F1) instrument at a heating (or cooling) rate of 10 ^{o}C min^{-1}. The highest occupied molecular orbital (HOMO) energy levels of target compound were measured on a CHI760D electrochemical workstation by using cyclic voltammetry (CV) with a glass carbon disk as the working electrode, a platinum wire as the counter electrode, a Ag/Ag^{+} (0.01 M of $AgNO_3$ in acetonitrile) as the reference electrode, and ferrocene as the standard reference. The material was dissolved in anhydrous dichloromethane solution with 0.1 mol/L Bu4NPF6 as the electrolyte to measure the oxidation, from which the HOMO energy level was estimated, whereas the lowest unoccupied molecular orbital (LUMO) energy levels were calculated by the difference between the band gap (E_g) evaluated from the onset of absorption spectra and HOMO energy level.

1.2. Device fabrication and measurement

Patterned indium-tin-oxide (ITO) glasses (Purchased from KINTEC Company, Hong Kong.)

with a sheet resistance of 20 Ω per square were ultrasonically treated in detergents and deionized water, then dried for 30 mins at 120 °C. After treated by oxygen plasma for 7 mins, Clean ITO substrates were transferred into the vacuum deposition system. When the pressure is less than 2×10^{-4} Pa, the devices were fabricated. The evaporation rates of organic materials, lithium fluoride (LiF) and aluminum (Al) were 1-1.5, 0.2 and 5-10 Å s^{-1} via a shadow mask, which were detected by a frequency counter and calibrated by a Dektak 6 M profiler (Veeco). The emitting area of the devices was determined by the overlap between ITO and Al electrodes. The current density–luminance–voltage characteristics were performed by the computer controlled Keithley 2450 Series Digital Source-meter and LS160 Luminancemeter (KONICAMINOLTA). EL spectra at different voltages were recorded by the optical analyzer FlAME-S-VIS-NIR photometer. Supposing the light emitted by OLEDs accorded with the Lambertian distribution, the EQEs can be calculated from the EL spectra, luminance, and current density.

1.3 Theoretical calculations

All the density functional theory (DFT) and time dependent DFT (TDDFT) calculations were carried out using Gaussian 09 package. The optimized ground-state geometries, energy levels, and frontier molecular orbital (FMO) distributions were calculated on the basis of DFT by using RB3LYP/6-31G(d, p) method. According to the TDDFT calculation, the optimized excited-state geometries, natural transition orbitals (NTOs), singlet and triplet state energies, and oscillator strength were performed by the RB3LYP/6-31G (d, p) level, and processed by Multiwfn.[1] Using the respective T_n geometries, spin−orbit coupling (SOC) matrix elements, $\langle S_1|\hat{H}SOC|T_n\rangle$, were calculated using a scalar relativistic TDDFT.

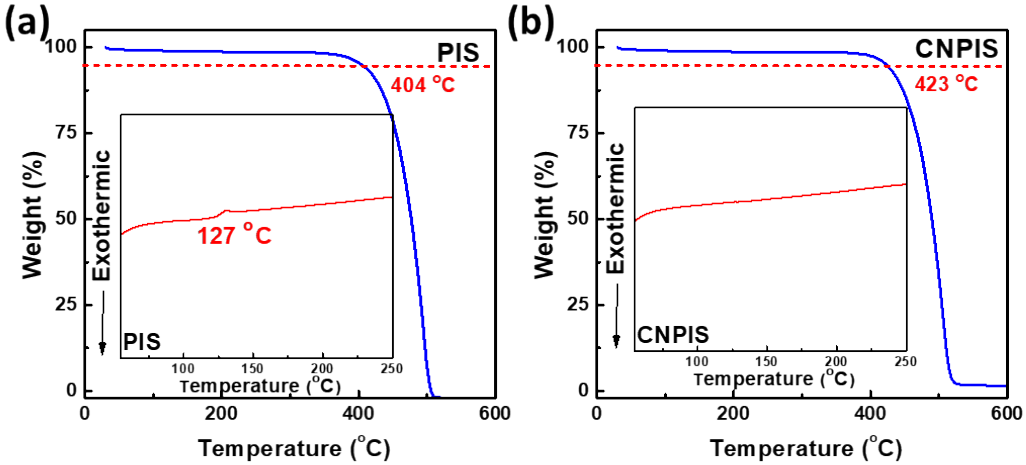

Figure S1. TGA thermograms of **PIS** (a) and **CNPIS** (b). Insert: DSC curves of **PIS** and **CNPIS**.

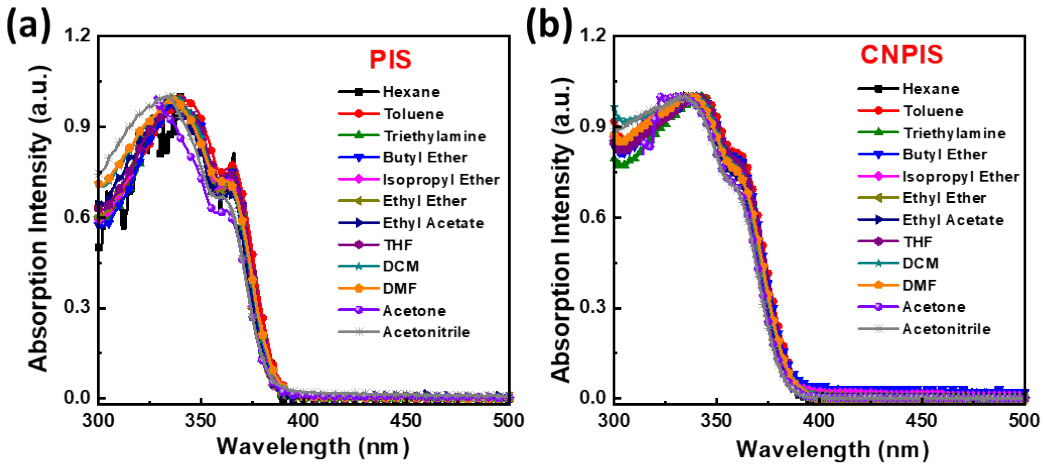

Figure S2. UV-vis absorption spectra of **PIS** and **CNPIS** in different solvents (10 uM) at room temperature.

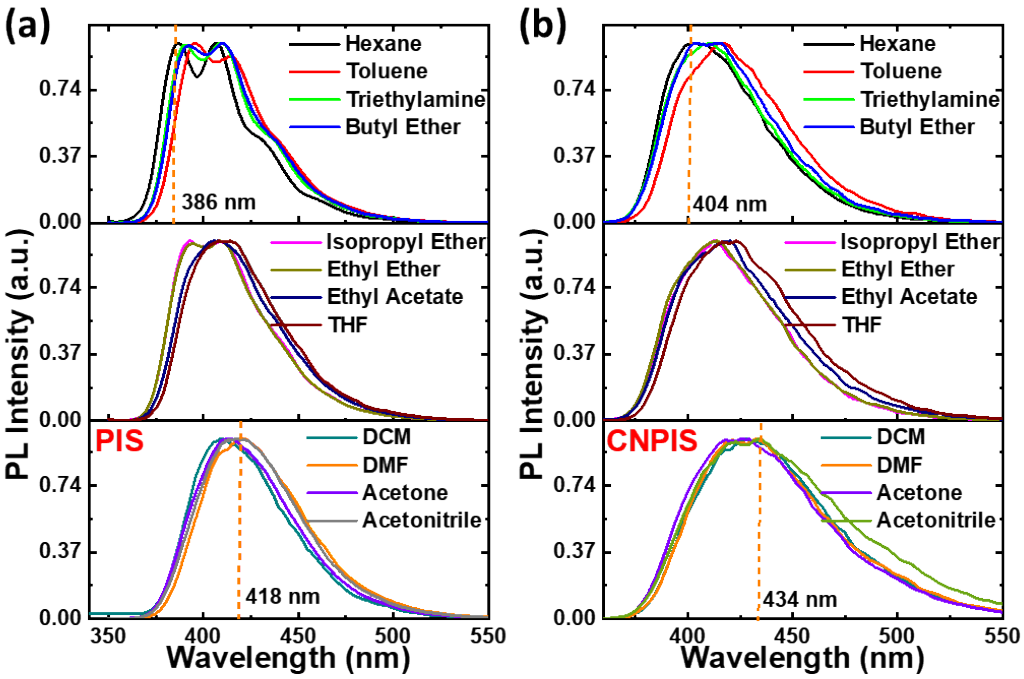

Figure S3. PL spectra of **PIS** and **CNPIS** in different solvents (10 uM) at room temperature.

Table S1. The detailed absorption and emission data of **PIS** in different solvents.

Solvents	**ε**	**n**	***f*(ε, n)**	**λ_a [nm]**	**λ_f [nm]**	**ν_a- ν_f [cm^{-1}]**
Hexane	1.9	1.375	0.0012	342	386	3333.03
Toluene	2.38	1.494	0.013	342	395	3923.31
Triethylamine	2.42	1.401	0.048	337	390	4032.56
Butyl ether	3.08	1.399	0.096	337	392	4163.39
Isopropyl ether	3.88	1.368	0.145	336	393	4316.61
Ethyl ether	4.34	1.352	0.167	336	395	4445.45
Ethyl acetate	6.02	1.372	0.2	333	405	5338.67
Tetrahydrofuran	7.58	1.407	0.21	337	408	5163.79
Dichloromethane	8.93	1.424	0.217	336	409	5312.03
Dimethylformamide	37	1.427	0.276	337	422	5976.91
Acetone	20.7	1.359	0.284	332	416	6082.02
Acetonitrile	37.5	1.344	0.305	328	418	6564.36

Table S2. The detailed absorption and emission data of **CNPIS** in different solvents.

Solvents	ε	n	f(ε, n)	λ_a [nm]	λ_f [nm]	ν_a- ν_f [cm^{-1}]
Hexane	1.9	1.375	0.0012	340	404	4659.29
Toluene	2.38	1.494	0.013	344	414	4915.18
Triethylamine	2.42	1.401	0.048	341	410	4935.27
Butyl ether	3.08	1.399	0.096	341	415	5229.13
Isopropyl ether	3.88	1.368	0.145	339	412	5226.68
Ethyl ether	4.34	1.352	0.167	337	414	5519.00
Ethyl acetate	6.02	1.372	0.2	336	420	5952.38
Tetrahydrofuran	7.58	1.407	0.21	340	423	5771.10
Dichloromethane	8.93	1.424	0.217	337	428	6309.10
Dimethylformamide	37	1.427	0.276	337	432	6525.44
Acetone	20.7	1.359	0.284	333	426	6555.85
Acetonitrile	37.5	1.344	0.305	334	434	6898.65

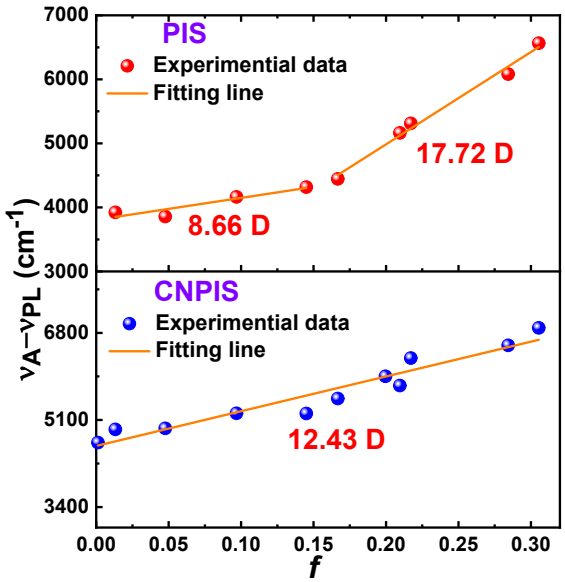

Figure S4. Solvatochromic Lippert-Mataga models of **PIS** and **CNPIS** with the Stokes shift (ν_a-ν_{PL}) as a function of solvent polarity (f).

Detailed Lippert-Mataga Calculation

The Stokes shift ($\nu_A - \nu_{PL}$) versus orientational polarizability ((ε, n)) of solvents can be constructed by the Lippert-Mataga model with the Equation 1 as below.

$$hc(\nu_A - \nu_{PL}) = hc(\nu_A^0 - \nu_{PL}^0) + \frac{2(\mu_e - \mu_g)^2}{a_0^3} f(\varepsilon,n) \quad (1)$$

Here, h is the Plank constant, c is the light speed in vacuum, μ_g and μ_e are the ground-state excited-state dipole moments, (ε, n) is the orientational polarizability of solvents, a_0 is the Onsager cavity radius, $\nu_A^0 - \nu_{PL}^0$ is the Stokes shifts when f is zero, respectively.

Take differential on both sides of the Equation 1, the Equation 2 can be obtained:

$$\mu_e = \mu_g + \{\frac{hca_0^3}{2} \times [\frac{d(\nu_A - \nu_{PL})}{df(\varepsilon,n)}]\}^{1/2} \quad (2)$$

(ε, n) and a_0 can be obtained by the Equation 3 and 4:

$$f(\varepsilon,n) = \frac{\varepsilon - 1}{2\varepsilon + 1} + \frac{n^2 - 1}{2n^2 + 1} \quad (3)$$

$$a_0 = (\frac{3M}{4\pi Nd})^{1/3} \quad (4)$$

Where, ε and n are dielectric constant and refractive index of solvent, N is Avogadro's number, M is molar mass, and d is density of the solvents, respectively. The values of (ε, n) and a_0 can be estimated by the Equation 3 and 4. The $\mu_g s$ of **PIS** and **CNPIS** (4.1426 and 1.1764 D) were estimated with the Gaussian 09 package at the level of B3LYP/6-31G(d, p). The $\frac{d(\nu_A - \nu_{PL})}{df(\varepsilon,n)}$ can be estimated with the solvatochromic experiment data listed in Table S1 and S2. With the information above, **PIS** shows two section lines with the μ_es of 8.66 and 17.72 D in low- and high-polar solvents, while the well-fitted linear relationship with the μ_e of 12.43 D was achieved based on **CNPIS**.

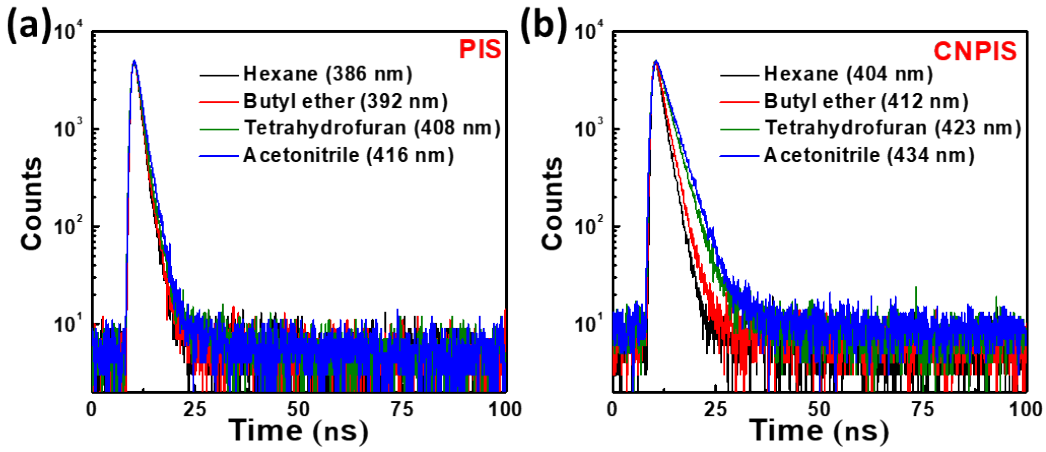

Figure S5. Transient PL decay spectra of **PIS** (a) and **CNPIS** (b) at hexane, butyl ether, tetrahydrofuran, and acetonitrile solutions (10 uM).

Table S3. PLQYs, lifetimes, radiative transition rates (k_r) and non-radiative transition rates (k_{nr}) of **PIS** and **CNPIS**.

	PIS				**CNPIS**			
	PLQY	τ [ns]	k_r[a] [$\times 10^8$ s^{-1}]	k_{nr}[b] [$\times 10^8$ s^{-1}]	PLQY	τ [ns]	k_r[a] [$\times 10^8$ s^{-1}]	k_{nr}[b] [$\times 10^8$ s^{-1}]
Hexane	0.764	1.33	5.74	1.77	0.450	1.74	2.59	3.16
Butyl ether	0.852	1.44	5.92	1.03	0.447	2.10	2.13	2.63
Tetrahydrofunan	0.858	1.65	5.20	0.86	0.253	2.86	0.88	2.61
Acetonitrile	0.922	1.73	5.33	0.45	0.062	3.16	0.20	2.97
Neat film	0.497	1.19	4.18	4.23	0.304	2.26	1.34	3.08

[a] $k_r = PLQY/\tau$; [b] $k_{nr} = 1/\tau - k_r$

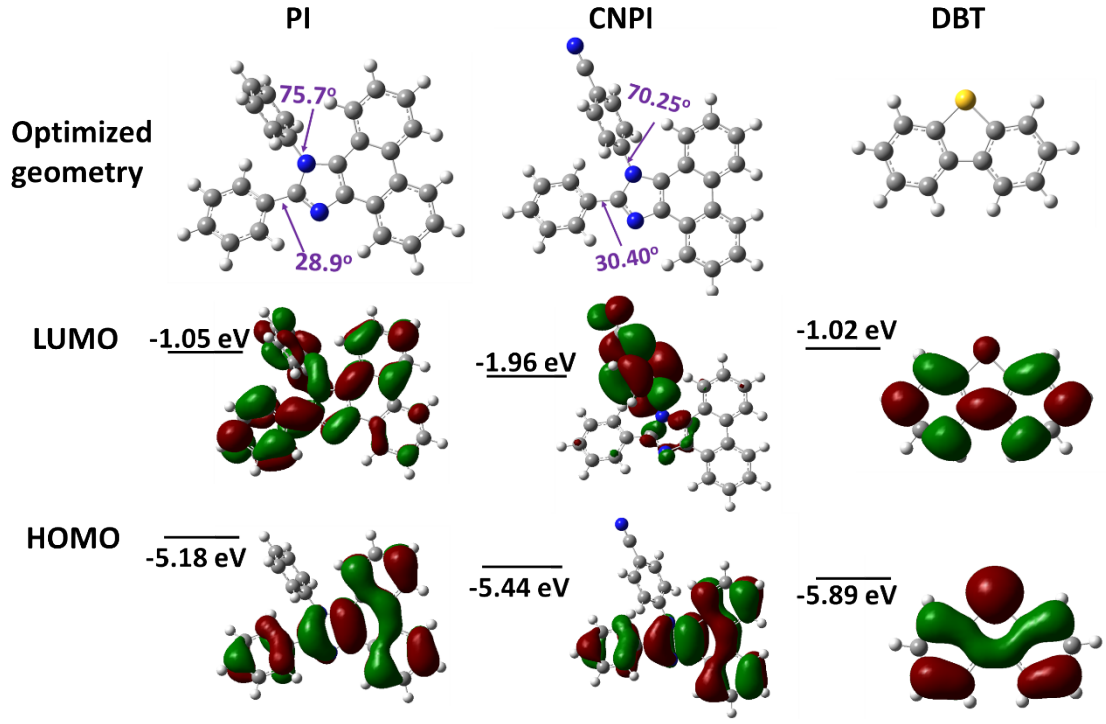

Figure S6. Optimized geometries and frontier molecular orbitals of the HOMO and LUMO of 1,2-diphenyl-1*H*-phenanthro[9,10-*d*]imidazole (PI), 4-(2-phenyl-1*H*-phenanthro[9,10-*d*]imidazol-1-yl)benzonitrile (CNPI), and dibenzothiophene (DBT), and their energy levels computed at the B3LYP/ 6-31G(d,p) level.

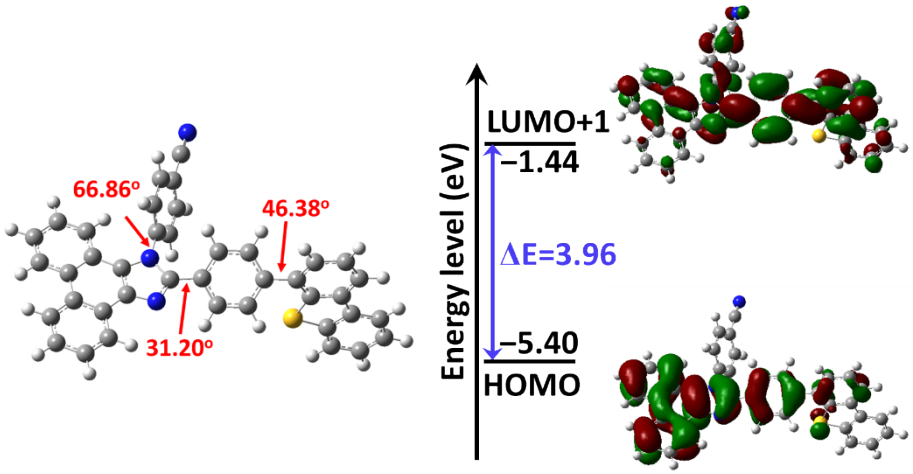

Figure S7. Optimized geometries and the HOMO and LUMO+1 distributions of **CNPIS**.

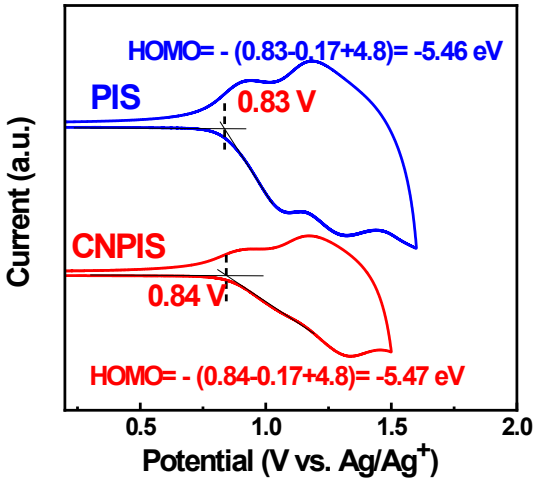

Figure S8. Cyclic voltammograms of **PIS** and **CNPIS** measured in anhydrous dichloromethane.

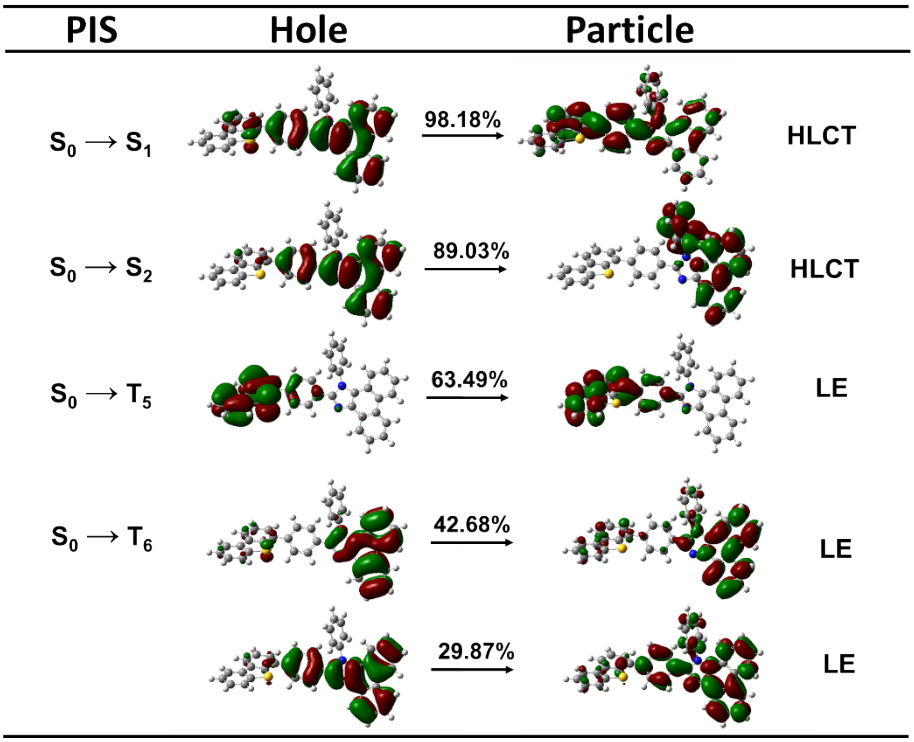

Figure S9. The calculated NTO distributions of singlet and triplet excited states (S_1, S_2, T_5, and T_6) of **PIS**.

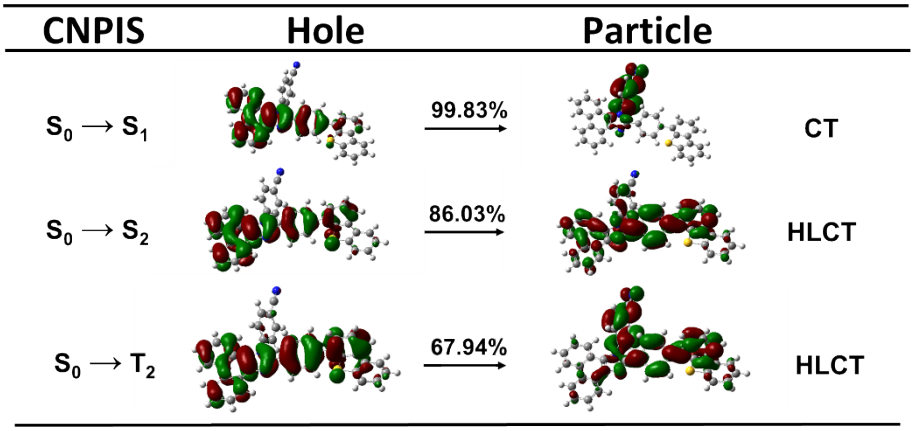

Figure S10. The calculated NTO distributions of singlet and triplet excited states (S_1, S_2, and T_2) of **CNPIS**.

Table S4. Energy levels of singlet and triplet states and oscillator strengths of singlet states of **PIS**.

Excited States	S energy level [eV]	T energy level [eV]	S Oscillator Strength
1	3.4565	2.6255	0.8318
2	3.7186	2.9631	0.0117
3	3.837	3.1542	0.0105
4	3.9178	3.3405	0.0076
5	3.9493	3.4184	0.0015
6	3.9678	3.5506	0.1291
7	4.0963	3.6761	0.01
8	4.2093	3.6899	0.0842
9	4.256	3.7907	0.0201
10	4.417	3.82	0.0564

Table S5. Energy levels of singlet and triplet states and oscillator strengths of singlet states of **CNPIS**.

Excited States	S energy level [eV]	T energy level [eV]	S Oscillator Strength
1	2.9154	2.5824	0.0312
2	3.5303	2.9392	0.6285
3	3.5567	3.0014	0.0113
4	3.6031	3.1732	0.0459
5	3.6491	3.2848	0.1581
6	3.8606	3.372	0.0058
7	3.8878	3.4166	0.0106
8	3.9297	3.5558	0.0032
9	4.0321	3.5806	0.0315
10	4.1398	3.5923	0.0098

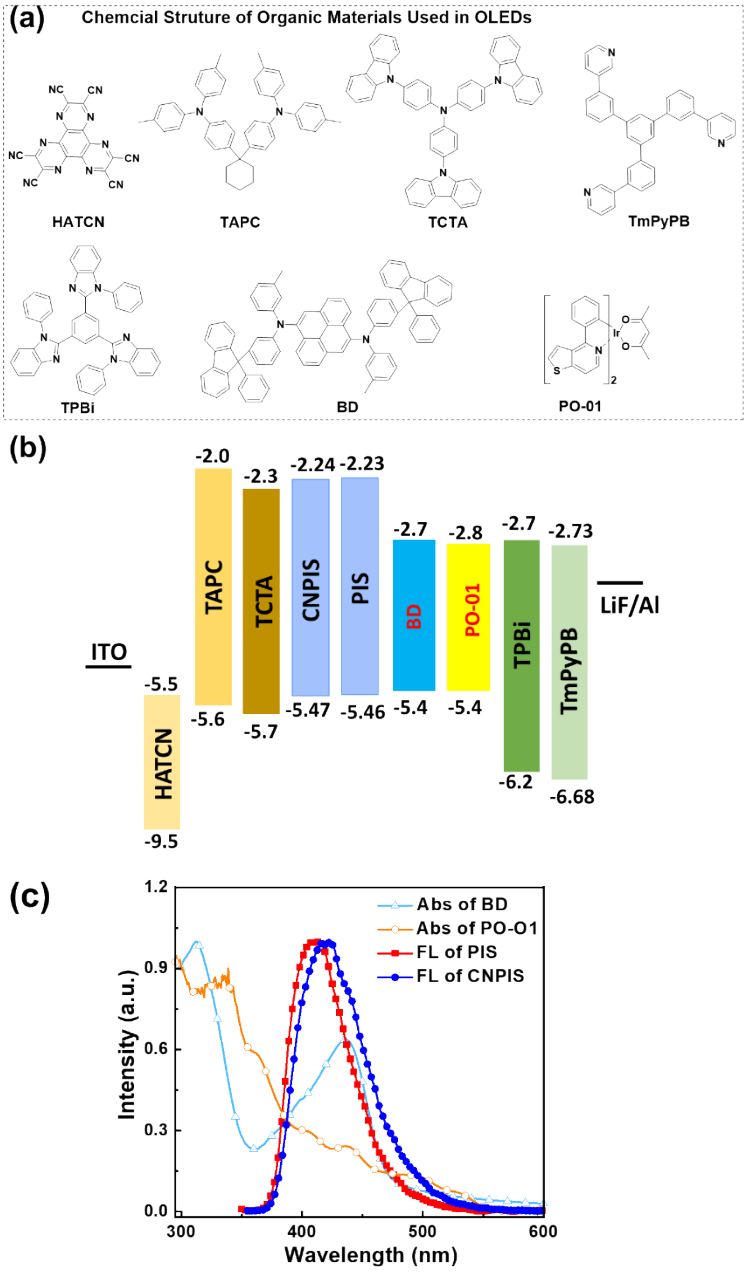

Figure S11. Chemical structures (a) and energy diagrams (b) of materials used in this work. (c) Ultraviolet-visible (UV-vis) absorption of materials **BD** and **PO-01**, and photoluminescence (PL) spectra of **PIS** and **CNPIS**.

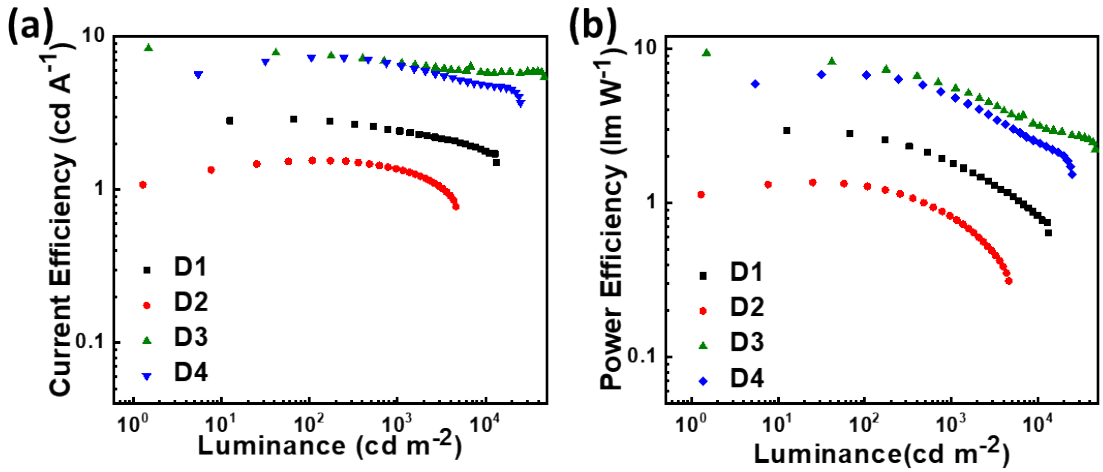

Figure S12. Current efficiency–luminance (a) and power efficiency-luminance (b) plots of the fabricated OLEDs (**D1**, **D2**, **D3**, and **D4**). The device structure is ITO/HATCN (10 nm)/TAPC (50 nm)/TCTA (10 nm)/ EML (20 nm)/TmPyPB (40 nm)/LiF (1 nm)/Al (100 nm), where EMLs are **PIS**, **CNPIS**, **PIS: 3wt% BD**, and **CNPIS: 3wt% BD** for **D1**, **D2**, **D3**, and **D4**, respectively.

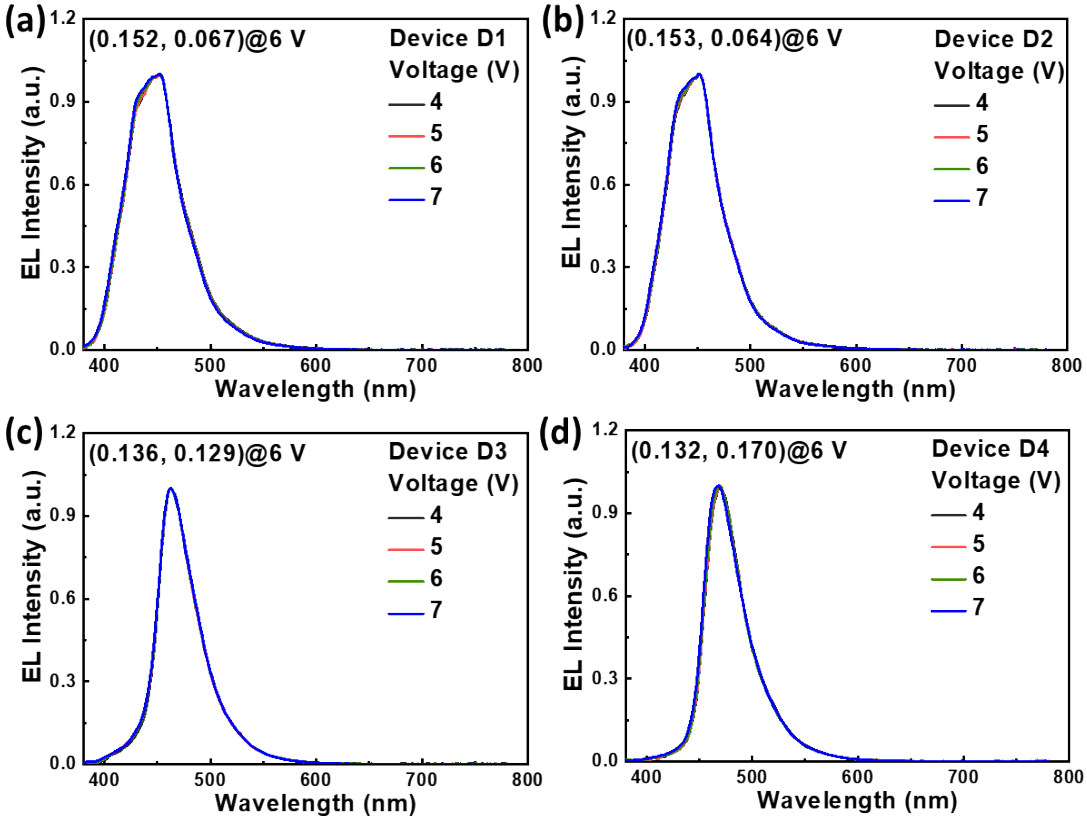

Figure S13. EL spectra at different applied voltages of the devices **D1** (a), **D2** (b), **D3** (c), and **D4** (d).

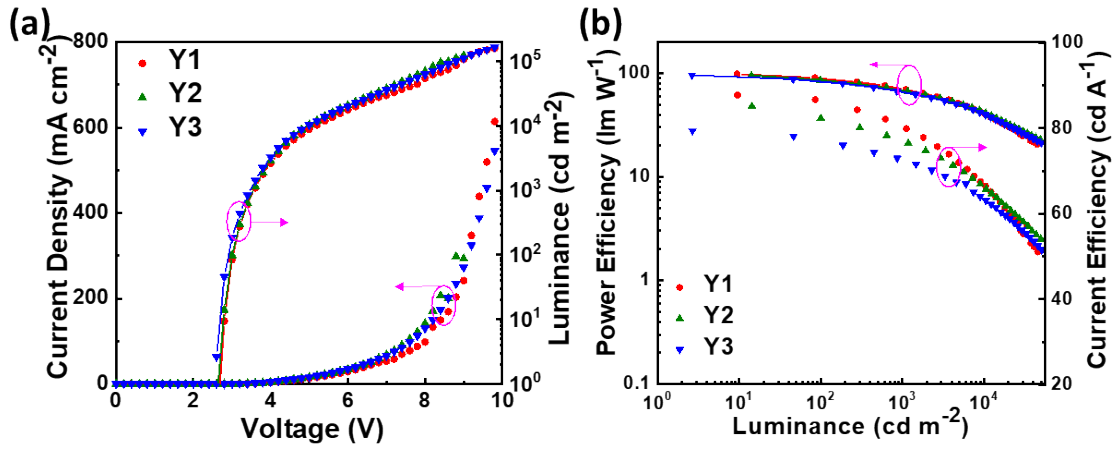

Figure S14. (a) Current-density–voltage–luminance characteristics of the orange OLEDs (**Y1**, **Y2** and **Y3**). (b) Power efficiency and current efficiency versus luminance curves of the orange OLEDs (**Y1**, **Y2** and **Y3**).

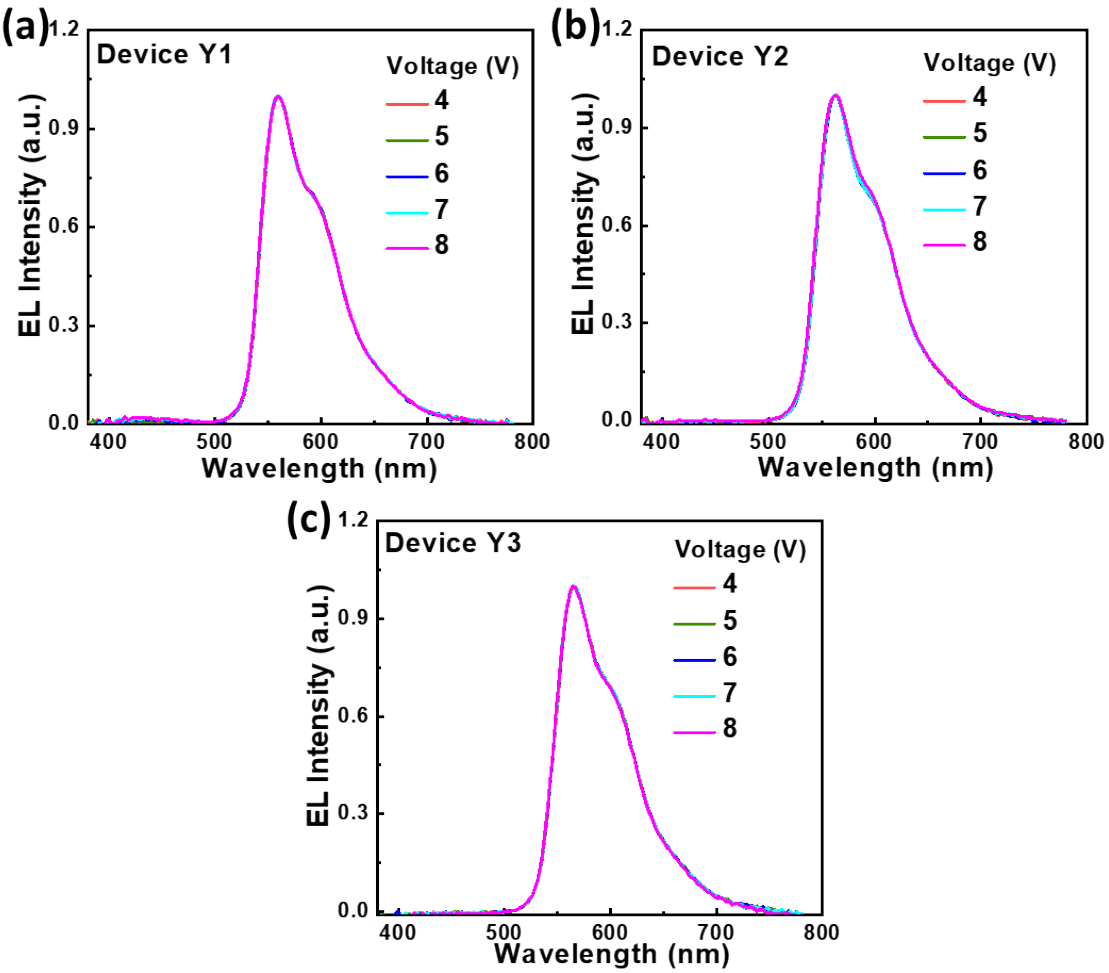

Figure S15. Normalized EL spectra at different applied voltages. (a) Yellow device **Y1**. (b) Yellow device **Y2**. (c) Yellow device **Y3**.

References

1. T. Lu, F. Chen, Multiwfn: A multifunctional wavefunction analyzer, *J. Comput. Chem.*, 2012, **33**, 580-592.